Acta Geodyn. Geomater., Vol. 22, No. 1 (217), 87–104, 2025
DOI: 10.13168/AGG.2025.0007
journal homepage: https://www.irsm.cas.cz/acta

ORIGINAL PAPER

PETROGENETIC STUDY OF DIORITE AND Fe-Mg DIORITE FROM THE SAMAR BAGH COMPLEX: INSIGHTS FROM PETROGRAPHIC AND GEOCHEMICAL ANALYSES

Farhat ULLAH [1], Matloob HUSSAIN [1], Syed Mamoon SIYAR [2,]*, Rehan KHAN [1], Abbas Ali NASEEM [1], Raham JALIL [3, 4], Fahad ALSHEHRI [5] and Muhammad SHAHAB [5]*

[1] *Department of Earth Sciences, Quaid-I-Azam University, Islamabad 45320, Pakistan*
[2] *Department of Geology, University of Malakand, Chakdara 18800, Pakistan*
[3] *School of Natural Sciences, Macquarie University, North Ryde 2109, Australia*
[4] *National Center of Excellence in Geology, University of Peshawar, Pakistan*
[5] *Abdullah Alrushaid Chair for Earth Science Remote Sensing Research, Geology and Geophysics Department, King Saud University, 2455, Riyadh 11451, Saudi Arabia*

**Corresponding author's e-mail:* mamoon280@yahoo.com; shahabgeo07@gmail.com

ARTICLE INFO

Article history:
Received 14 November 2024
Accepted 18 March 2025
Available online 26 March 2025

Keywords:
Kohistan Island Arc
Petrogenesis
Kamila Amphibolite Belt
Diorite
Fe-Mg Diorite
Himalayan Orogeny
Petrography
Geochemistry

ABSTRACT

This study presents petrographic and geochemical investigations, in conjunction with field observations of the diorite and Fe-Mg diorite of the Samar Bagh Complex, located in the north-western part of the Kamila Amphibolite Belt in Northern Pakistan. The field investigations classify these rocks into dark grey to brownish diorite having quartz veins, alternating sheared and compacted zones, dark brown Fe-Mg diorite consisting of azurite and malachite, quartz veins, and oxidation of quartz veins in association with copper ores. The petrographic observations indicate these rocks primarily consist of plagioclase, clinopyroxene, amphiboles, quartz, alkali feldspar, magnetite, hornblende, biotite, sericite, olivine, orthopyroxene, hematite, and minor flakes of muscovite. The geochemical discrimination plots indicate tholeiitic magma series, with the ferron nature for diorite and magnesium-rich traits for Fe-Mg diorite. The tectonic classification of the Samar Bagh Complex, with rocks ranging from peraluminous to metaluminous, indicates that diorite, Fe-Mg diorite in mantle fractionates, island arc, and continental arc origins. This high-potassium to low-potassium rock is linked with the early intraoceanic subduction of the Neo-Tethys beneath the Asian Plate, intrusion of the Chilas Complex, interaction of the Indian Plate and the Kohistan Island Arc, resulting in the formation of diorite, Fe-Mg diorite, granodiorite, porphyry quartz monzonite, monzonite, and trachy andesite respectively. These findings contribute to the understanding of the magmatic and tectonic evaluation of the unsolved questions regarding the intermediate to felsic portion of the Kamila Amphibolite Belt.

1. INTRODUCTION

The Himalayan Orogeny is a comprehensive model of the complex history of crustal evolution and a diverse geological environment. It has been characterized into three main geological units: the Indian Plate, Kohistan Island Arc (KIA), and Eurasian Plate (Gibbons, 2015; Shahab et al., 2025). The KIA is one of the complete oceanic section, comprising rocks from the mantle to the upper crust (Rehman et al., 2011). This remarkable natural laboratory comprises amphibolites, calc-alkaline intrusions, mafic-ultramafic complexes, volcanic, and volcanic sedimentary rocks (Petterson, 2010).

The Kamila Amphibolite Belt is the most basic unit of KIA and is exposed along the Main Mantle Thrust (MMT). It stretches from Nanga Parbat to Afghanistan in the west through Dir, Bajaur, and Babusar top through Asmar Valley (Khan et al., 2012). The length of this belt is 350 km and the width ranges from 10 to 50 km. The Kamila Amphibolite Belt is further divided into banded amphibolites and non-banded amphibolites. The banded amphibolites are derived from the volcanic and plutonic antecedents, whereas the non-banded are derived from plutonic rocks (Jan, 1990). This amphibolite belt has a complex set of lithologies. The dominant lithology is amphibolite, which is fine to medium-grained in the eastern part of the belt and medium to coarse-grained in the western section of the Kamila Amphibolite Belt (Khan et al., 1993; Jan, 1990). In addition to the amphibolites that predominate in the belt, a wide range of other rocks having small to large bodies can also be found which includes granites, granodiorites, dunites, diorites, peridotites, pyroxenites, hornblendites, granitic pegmatites, hornblende pegmatites, aplites, olivine gabbros, and meta pillows (Jan, 1990). The petrogenesis of this belt is complex due to the nature of some plutonic rocks that predate amphibolites. It is also uncertain whether the ultramafic to intermediate rocks represent the intrusions and cumulates from the KIA lower layers. The granitic lithologies present in the belts may be due to partial melting of the

Cite this article as: Ullah F, Hussain M, Siyar S M, Khan R, Naseem AA, Jalil R, Alshehri F, Shahab M: Petrographic study of Diorite and Fe-Mg Diorite from the Samar Bagh Complex: Insights from petrographic and geochemical analyses. Acta Geodyn. Geomater., 22, No. 1 (217), 87–104, 2025. DOI: 10.13168/AGG.2025.0007

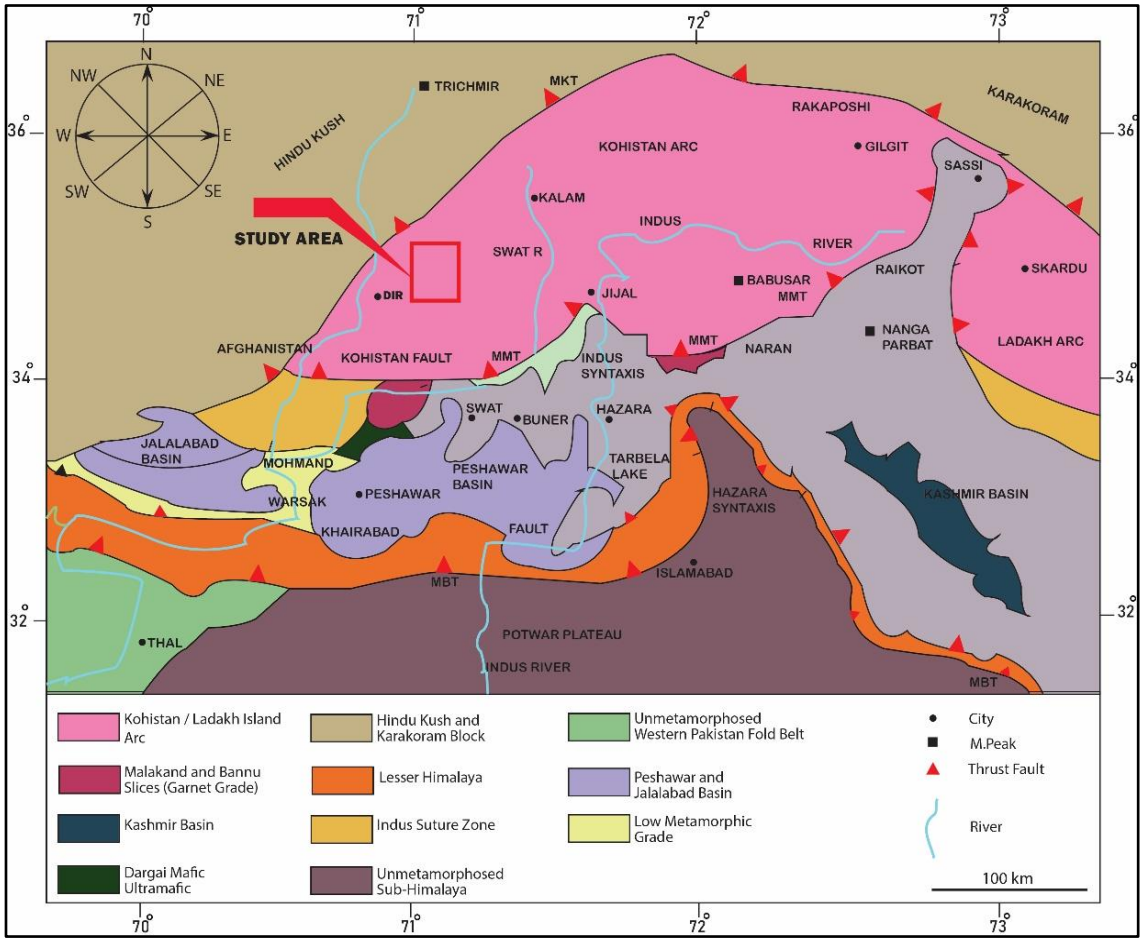

Fig. 1 Geological map of North-Western Himalayas, showing study area marked by red rectangle (Modified after Ahmad et al., 2003).

amphibolites during melting (Jan, 1990). In conclusion, there are still a lot of unsolved questions about the Kamila Amphibolite Belt exposed in Northwestern Pakistan. The intricate petrology and structure of the rocks necessitate precise geological mapping, age determination, and geochemistry (Jan, 1990).

The study area has been studied by Kakar et al., (1973) and named the Jandul Valley rocks, part of the Kamila Amphibolite Belt. Later, Sarwar (1997) divided the Kamila Amphibolite Belt into the Tora Tigga Complex, Timergara Complex and Samar Bagh Complex in the Dir area. The petrogenetic study of the Samar Bagh Complex is not fully comprehended, this study aims to fill these gaps by conducting multiple approaches, including field observations and petrography in conjunction with geochemical analysis**.**

2. GEOLOGY AND TECTONICS

Kohistan, an intra-oceanic arc, formed due to the India-Asia collision-related tectonics (Zafar et al., 2019b, 2025; Nakazawa et al., 2020). The most prominent members of the Kohistan Island Arc exposed at Dir Lower include the Kohistan Batholith, Kamila Amphibolite Belt, and Dir Volcanics Group (Petterson, 2019; Jan, 1990). The Kohistan Batholith is a basic geological unit of the KIA, which is 300 km long and 60 km wide (Petterson, 2019; Khan, 1993). The Kohistan Batholith consists of gabbro, hornblendite, diorite, quartz diorite, granodiorite, granite, pegmatite and aplite (Zafar et al., 2023, 2021; Searle et al., 1999). Many rocks of the batholith show a common calc-alkaline trend origin, but some of the rest have tholeiitic, subalkaline or alkaline origin (Ali et al., 2024; Petterson and Windley, 1991). The Kamila Amphibolite Belt is one of the major portions of the southern part of the KIA (Zafar et al., 2020b; Khan et al., 1993). The Kamila Amphibolite Belt is 250 km long and 10-45 km wide. The Kamila Amphibolite Belt boundary is defined by the Indus Tsangpo Suture Zone or the Jijal Complex to the south and the Chilas Complex to the north (Zafar et al., 2024; Ali et al., 2021; Khan et al., 1997). Dir Volcanics Group is a 120 km long and 15-20 km wide belt that runs through Dir-Swat Valley in Western Kohistan (Petterson, 2010). The Dir Volcanics Group is further divided into the Baraual Banda Slate Formation and Utror Volcanic Formation (Khaliq, 1991). The thickness of the Baraual Banda Slate Formation is about 3 km. The lower part of this formation contains conglomerates, breccia, and pebbly sandstone, while the upper part consists of thin

bedded sandstone, siltstone and mudstone (Sullivian et al., 1993). Rare interbedded limestone in Baraual Banda Slate Formation contains the marine faunas of the Late Paleocene age (Sullivian et al., 1993). The Dir Utror Formation comprises basalt, basaltic andesite, dacite, rhyolite, pyroclastic breccia and calc-alkaline nature volcanic tuff (Shah et al., 1994; Majid et al., 1981; Majid and Paracha, 1980).

It is widely documented that plutonic rocks such as granitioids are important to understand the magmatic sources and tectonic histories (Zafar et al., 2019a, 2019b, 2020a; Rehman et al., 2021). The Samar Bagh Complex is located north of the Mantle Main Thrust (MMT) and is mainly composed of plutonic, and volcanic rocks, which is part of the northwestern stretching of the southern part of the Kamila Amphibolite Belt (Jan, 1990). The plutonic rocks consist of granodiorites, diorites, Fe-Mg diorites, porphyry quartz monzonites, and monzonites. The volcanic rocks contain andesitic and dacitic tuffaceous rocks. This work is the first basic work on the intermediate to felsic rocks of the Kamila Amphibolite Belt exposed at Dir Lower and extended to Afghanistan. The present research will help to solve the various unsolved questions regarding the intermediate to felsic magma source of this belt. This work can be aligned with the recommendations of (Jan, 1990) which suggest that petrology, geological mapping, and geochemistry are necessary to solve the mystery of granitic composition in this amphibolite belt.

3. MATERIALS AND METHODS

3.1. FIELD OBSERVATIONS

The diorite of the Shahi Khel area is a large, prominent body of the Samar Bagh Complex. These diorites are coarse grained with minor color variations with no fractures. The fresh surface color of the rocks is grayish, while light brown to dark brown on weathered surfaces with compact and hard nature, having recorded alternate zones of weathering (Figs. 2b, 2c). Veins are present of different sizes, ranging from small thin to large thick. The principal composition of the veins is quartz, feldspar, muscovite, and some traces of biotite. The Kakas Maskini Fe-Mg Diorites are dark grayish color in fresh and brownish color on weathered surfaces (Figs. 2d, 2e). The Kakas Maskini Fe-Mg Diorite has copper mineralization (the blue is azurite, the green is malachite) present at 34°58′29″ N and 71°33′45″ E (Fig. 2f). The quartz feldspathic dykes are also present, and in some portions these dykes and the accumulation of quartz show oxidation due to copper mineralization (Fig. 2f).

3.2. LABORATORY WORK

Detailed fieldwork was conducted in the study area for field investigations, collection of rock samples for thin section preparation, and geochemical analysis. Thin sections were prepared at the Rock Cutting Laboratory of Bacha Khan University Charsadda, Pakistan, and were studied at the Sedimentology Laboratory, National Center of Excellence in Geology (NCEG), University of Peshawar. The grinding of rock samples for X-ray fluorescence and XRF analysis were carried out in the Rock Cutting Laboratory, at Centralized Resources Laboratory (CRL) University of Peshawar.

3.2.1. PETROGRAPHY

Following up the field investigations, a total of 14 rock samples were selected for thin section and x-ray fluorescence analyses. The standard operating procedure of thin section preparation was followed with a suitable, selective, and interested portions of the rock samples cut with the help of a rock cutting machine. The cut rocks samples are then ground with 120 grit carborundum followed by 240 grit 400 and 600 grit to reduce thier width. After grinding, the rock sam ples are then glued with a glass slide with the help of epoxy. The process of grinding is repeated to reduce the thickness further using up to 600 grit, after the 600 grit the polishing stage starts, and the thin section is ground with 800 and 1000 grit. Continuously check the thinness of the thin section to avoid any breakage or loss of rocks due to grinding. The grinding continued until the thin sections were polished and ordinary light passed from it. The prepared thin sections were examined using a Nickon LV100ND Polarizing Microscope and photomicrographs were captured.

3.2.2. X-RAY FLUORESCENCE

The selected samples for X-ray fluorescence were powdered in order to provide a uniform and smooth surface, necessary for accurate measurements. The analysis was carried out using an XRF spectrometer EDX-7000. The powdered samples were placed in polypropylene cups having surrounding atmosphere air in the XRF chamber and exposed to an x-ray spectrometer, with a collimator of 10 mm, causing the emissions of characteristic fluorescence from the element present. This emitted radiation was detected and analyzed to determine the major and minor elements.

4. RESULTS

4.1. PETROGRAPHIC OBSERVATIONS

4.1.1. SHAHI KHEL DIORITE

The petrographic observation the Shahi Khel Diorite reveal that plagioclase, clinopyroxene, amphiboles, and biotite are the dominant minerals having sufficient concentrations of quartz, alkali feldspar, olivine, and magnetite with minor amounts of orthopyroxenes, sericite, and traces of muscovites (Figs. 3a-3d). Texturally, the rock is coarse-grained with a sufficient amount of dark colored minerals. The plagioclase is the most common mineral in the studied thin section recorded concentrations from 78 % to 87 % (Table 1). The observed features of this

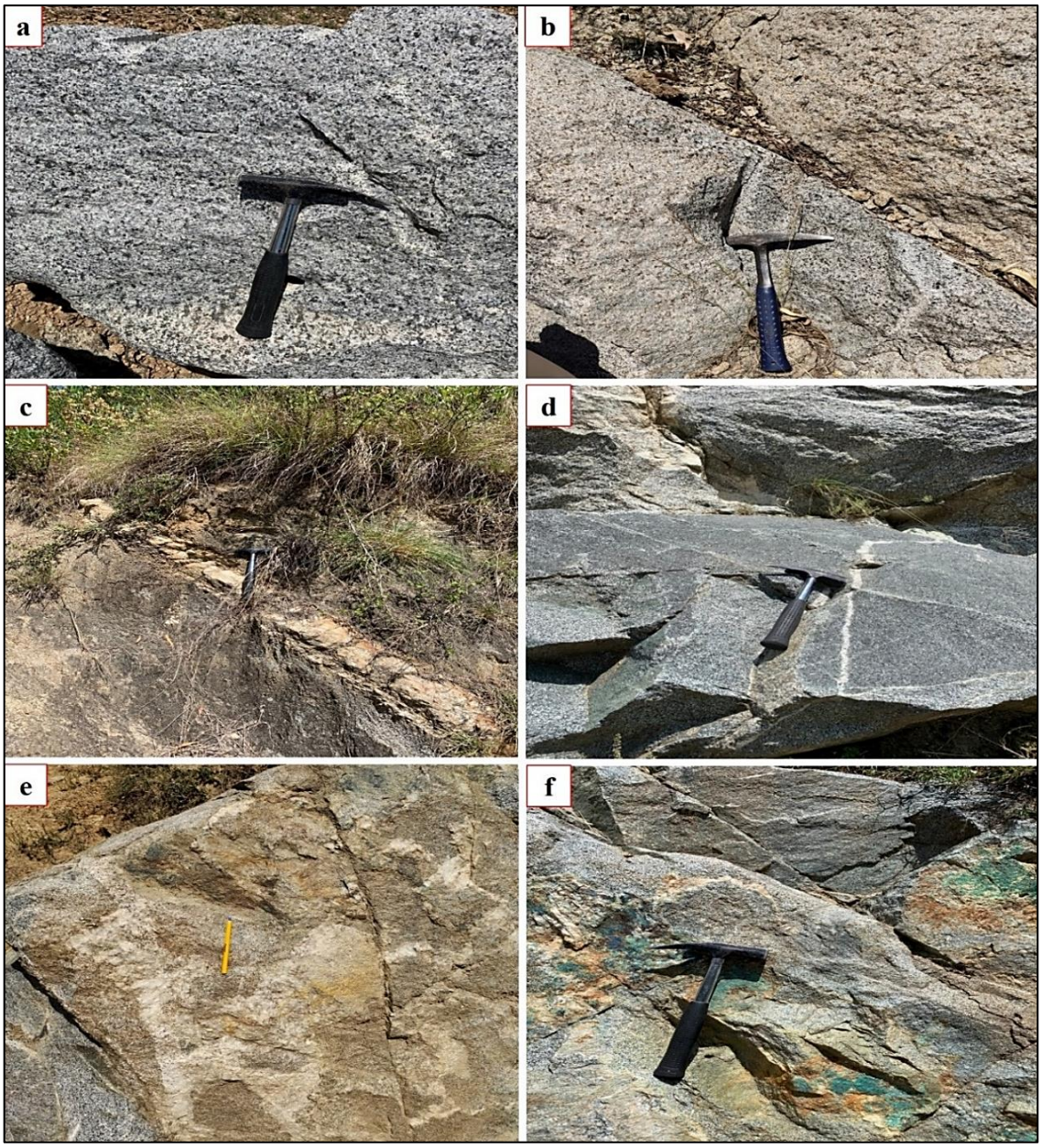

Fig. 2 Outcrops showing (**a**) fresh surface of Shahi Khel Diorite (**b**) alternate weathered and fresh surfaces of Shahi Khel Diorite (**c**) quartz veins in Shahi Khel Diorite (**d**) fresh surface of Kakas Maskini Fe-Mg Diorite having quartz vein (**e**) weathered surface of Kakas Maskini Fe-Mg Diorite having quartz veins (**f**) copper ores with oxidation of quartz veins on close examination.

plagioclase bulk are subhedral to anhedral crystal form, cleavages, and several types of twining (Carlsbad twinning and Polysynthetic twining) (Figs. 3a, 3d).

The minor amount of disseminated quartz is recorded in thin sections ranges from 0.5 % to 2 % having inclusion in clinopyroxene (Table 1, Fig. 3c). The alkali feldspar is an important member of QAP classification records its minute concentrations from 0.5 % to 1.5 % and observed in association with muscovite (Table 1, Fig. 3c). The amphibole series minerals are the prominent minerals encountered during microscopic study having concentration of 7 % to 10 % with several sets of cleavages observed (Table 1, Fig. 3b).

The dark brown hornblende is an inclusion in clinopyroxene was noticed. The clinopyroxene has well-defined concentrations ranging from 5 % to 10 % (Table 1, Fig. 3c). The augite is the most prominent member of clinopyroxene, occurring as a single large crystal with cleavages (Table 1, Fig. 3b). The sufficient concentration of biotite ranges from 5 % to 10 % having a dark grey to black color (Table 1, Fig. 3d). The dark black color magnetite is observed with its characteristics patterns ranges from 1 % to 3 % as illustrated in Table 1. The olivine mineral is also

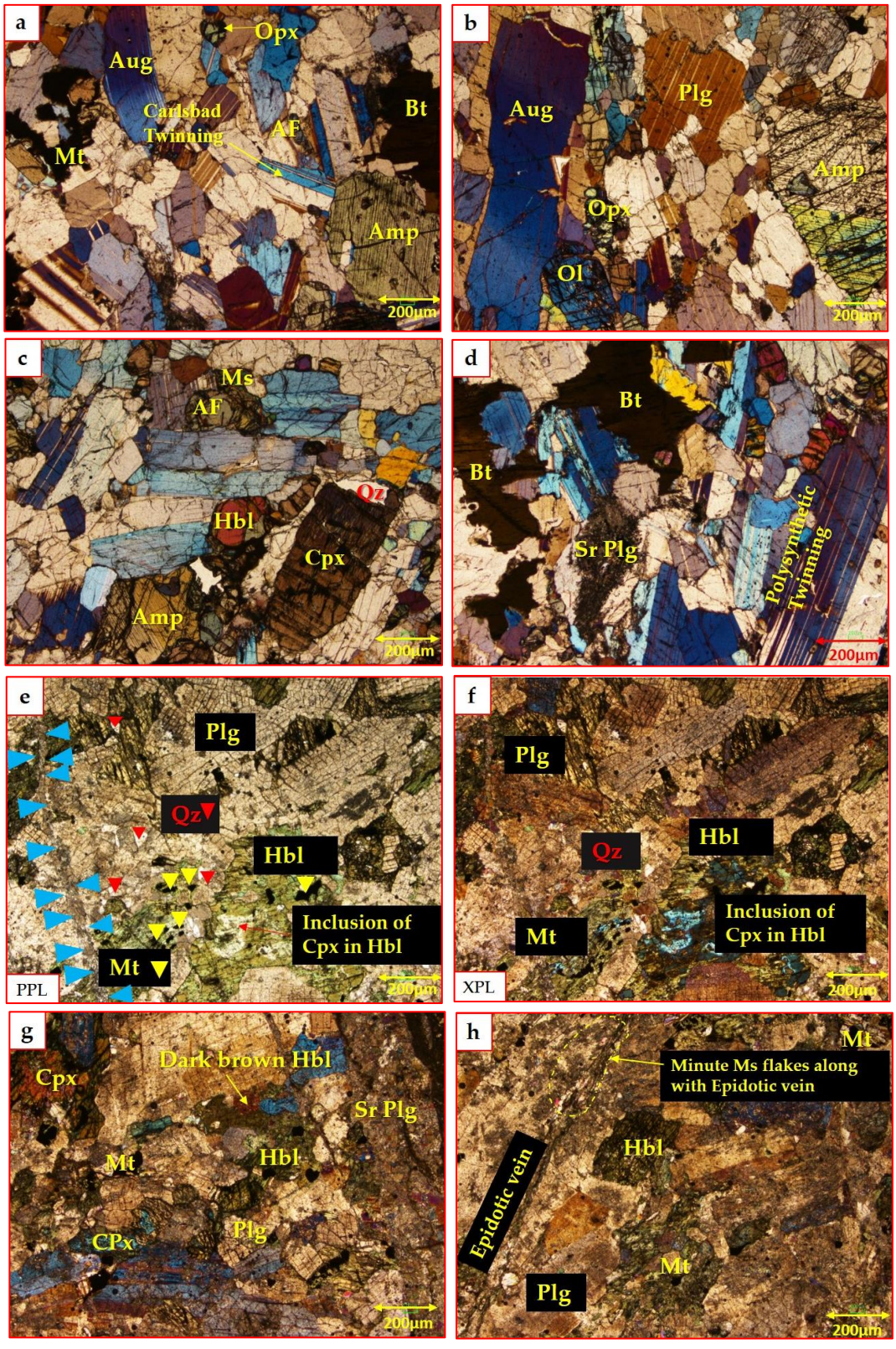

Fig. 3 Photomicrographs illustrating (**a**) assemblages of plagioclase having carlsbad twinning, alkali feldspar, quartz, amphibole, biotite, magnetite, and augite (**b**) the plagioclase with a large crystal of augite, olivine, and amphibole (**c**) the assemblages of plagioclase, alkali feldspar, quartz, amphibole, and clinopyroxene having inclusion of fresh quartz (**d**) the polysynthetic twinning in plagioclase and Sericitized plagioclase, having large crystals of biotite, magnetite, and augite (**e**) the assemblages of plagioclase, disseminated minor quartz crystals, magnetite pattern in hornblende and inclusion of clinopyroxene in hornblende with the epidotic veins (PPL) (**f**) the assemblages of plagioclase, disseminated minor quartz crystals, magnetite pattern in hornblende and inclusion of clinopyroxene in hornblende (XPL) (**g**) the sericitized plagioclase and dark brown hornblende (**h**) photomicrograph showing the assemblages of plagioclase having epidotic veins and association of mica flakes. (**Key**: Plg; Plagioclase, Sr Plg; Sericitized Plagioclase, Qtz; Quartz AF; Alkali-Feldspar, Orth; Orthoclase, Bt; Biotite, Ms; Muscovite, Aug; Augite, Amp; Amphibole, Hbl; Hornblende, Cpx; Clinopyroxene, Opx; Orthopyroxene, Mg; Magnetite, Ol; Olivine, Ht; Hematite).

Table 1 Model mineralogical composition of Shahi Khel Diorite and Kakas Maskini Fe-Mg diorite.

Rock Type	Sample	Plg	Qz	AF	Amp	Cpx	Opx	Bt	Ms	Ol	Mg	Ht	Sr
	SG-1	77	1	1	6	5	1	5	1	-	3	-	-
	SG-3	79.5	2	1.5	7	10	-	-	-	-	-	-	-
	SG-5	75	0.5	-	10	10	-	-	-	1.5	-	-	3
	SG-7	87	0.5	0.5	-	-	-	9.5	2	1	-	-	-
Diorite	SG-8	76	1.5	1	5	6.5	1.5	5.5	0.5	-	1	-	1.5
	SG-10	74.5	1.5	2.5	6.5	5	-	6.5	-	-	0.5	-	
	SG-12	73	2	1	8	9	-	5	-	1	1	-	-
	SG-15	76.5	1.5	1	9	8	-	3	-	1	-	-	-
	KK-1	73	2	-	15	5	-	-	-	-	4	-	1
	KK-2	69.5	1	-	17	7	-	-	-	-	5	-	0.5
Fe-Mg	KK-3	75	1	-	8	9	-	-	-	-	7	-	-
Diorite	KK-4	80	3	-	10	4	-	-	-	-	2	-	0.5
	KK-5	77	2.5	0.5	10.5	5	-	-	-	-	4.5	-	-
	KK-6	78.5	2	0.5	9.5	5.5	-	-	-	-	3.5	-	0.5

observed in thin section study with the amount of 1 % to 1.5 % having cleavages (Table 1). Sericite, the alteration product of plagioclase can be seen in the thin section with a concentration of 3 % (Table 1, Fig. 3d). The orthopyroxenes and muscovite having concentrations of 1% were recorded in the thin section (Table 1).

4.1.2. KAKAS MASKINI FE-MG DIORITE

The representative samples of Kakas Maskini Fe-Mg Diorite show a high concentration of plagioclase, hornblende, clinopyroxene, and magnetite with lesser amounts of quartz, sericite, and traces of alkali feldspar and flakes of muscovite (Figs. 3e-3h). The plagioclase shows concentration from 69.5 % to 80 %, having cleavages and partial sericitization of plagioclase with epidotic veins (Table 1, Figs. 3e, 3f). The trace flakes of muscovite are observed at close interpretation along the epidotic veins (Fig. 3h). The sericitization of plagioclase is subject to hydrothermal alteration. A minor amount of quartz is also observed with a disseminated and widespread nature in the thin sections with subhedral crystal form and an estimated percentage of concentration ranges from 1 % to 3 % (Table 1, Fig. 3e). The hornblende is the most prominent member of these diorites, with concentrations of 8 % to 17 % having some weathering and inclusion of clinopyroxene (Table 1, Figs. 3e, 3f). The dark brown hornblende is also recorded (Fig. 3g). The concentration of clinopyroxene ranges from 4 % to 9 % (Table 1). The clinopyroxene minerals show inclusions in hornblende groundmass are subhedral to anhedral having cleavages (Fig. 3g).

Magnetite is the next most important dissiminated mineral encountered in petrographic observation ranging from 2 % to 7 % (Table 1). The close examination study reveals that magnetite is mostly associated and developed a specific pattern with hornblende minerals (Fig. 3e). The magnetite crystals are mostly subhedral in nature. This shows that the magnetite crystal has enough time for cooling and development within the hornblende (Fig. 3e). The hydrothermal alteration product sericite was recorded in the Fe-Mg diorite with a concentration of 0.5 % to 1 % (Table 1, Fig. 3g). The Fe-Mg diorite samples also contain minor flakes of muscovite (Fig. 3h). The model mineralogical composition of Shah Khel Diorite and Kakas Maskini Fe-Mg Diorite are enlisted in Table 1, and their representative position in IUGS plutonic plot is illustrated in Figure 4.

4.2. GEOCHEMISTRY

4.2.1. MAJOR OXIDES GEOCHEMSITRY

The Shahi Khel Diorite is intermediate in nature having the SiO_2 content from 55.7 % to 59.5 %, followed by Al_2O_3 composition ranging from 22.14 % to 24.07 %, CaO 8.03 % to 8.67 %, Fe_2O_3 5.5 % to 6.22 %, Na_2O 2.98 % to 3.67 %, TiO_2 0.4 % to 0.52 % MgO 0.2 % to 0.47 %, MnO 0.1 % to 0.12 %, K_2O 0.6 % to 0.77 % and P_2O_5 0 % respectively (Table 2). The Kakas Maskini Fe-Mg Diorite contains SiO_2 content from 55.2 % to 55.8 %, followed by Al_2O_3 composition ranging from 17.92 % to 18.88 %, CaO 5.36 % to 5.67 %, Fe_2O_3 9.89 % to 9.26 %, Na_2O 1.37 % to 1.71 %, TiO_2 0.65 % to 0.8 3 %, MgO 9.46 % to 10.03 %, MnO 0.1 % to 0.14 %, K_2O 0.57 to 0.71 % and P_2O_5 0 % respectively as shown in Table 2. The Fe-Mg diorite of Kakas Maskini area is different from Shahi Khel Diorite in terms of Mg and Fe variations, SiO_2, Na_2O, CaO, and K_2O largely. The average concentration of Fe_2O_3, MgO, Al_2O_3, Na_2O, CaO, and K_2O of Fe-Mg diorite of the Kakas Maskini area are higher than the Fe_2O_3, MgO, Na_2O, CaO, and K_2O of Shahi Khel Diorite while, lower in concentration of SiO_2, Al_2O_3 as compared to Shahi Khel Diorite (Table 2).

4.2.2. ROCK CLASSIFICATION DIAGRAM

In the total Alkali silica diagrams for plutonic rocks (SiO_2 vs Na_2O+K_2O) of Cox et al. (1979), the studied samples of Shahi Khel Diorite and Kakas Maskini Fe-Mg Diorite plot within the diorite geochemical boundary (Fig. 5).

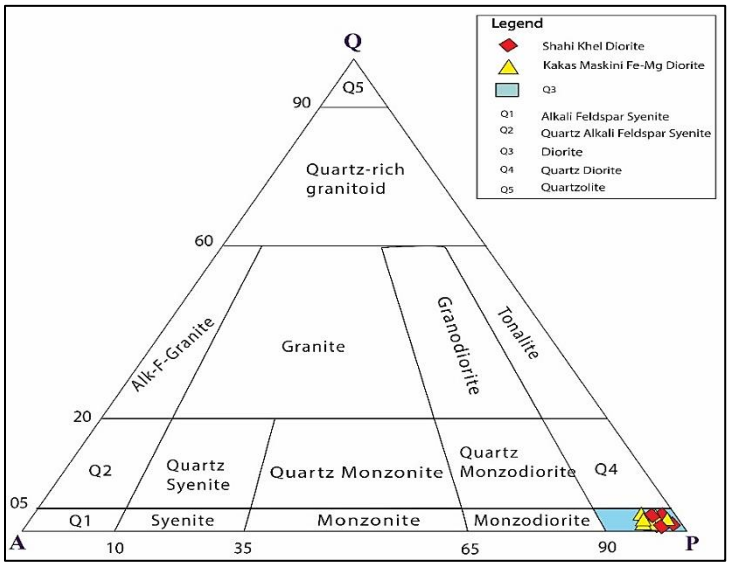

Fig. 4 Model mineralogical composition of the Shahi Khel Diorite and Kakas Maskini Fe-Mg Diorite plotted on the IUGS classification diagram (Le Maitre, 2002).

Table 2 Major oxide data from geochemical analysis of the Shahi Khel Diorite and Kakas Maskini Fe-Mg Diorite.

Rock Type	Sample	SiO_2	TiO_2	Al_2O_3	Fe_2O_3	MnO	MgO	CaO	Na_2O	K_2O	P_2O_5
Diorite	SG-1	58.31	0.52	24.04	5.5	0.1	0.32	8.1	3.35	0.69	0
	SG-3	58.6	0.36	24.17	6.01	0.1	0.21	8.43	3.67	0.60	0
	SG-5	59.5	0.56	23.53	6.23	0.12	0.41	8.63	2.92	0.77	0
	SG-7	59.7	0.4	23.04	5.96	0.1	0.20	8.4	3.33	0.69	0
	SG-8	59.4	0.3	22.91	5.73	0.12	0.34	8.03	3.01	0.71	0
	SG-10	58.24	0.32	22.14	6.16	0.11	0.34	8.46	3.32	0.69	0
	SG-12	58.33	0.48	22.22	6.22	0.11	0.32	8.67	3.08	0.63	0
	SG-15	57.7	0.5	24.04	5.45	0.11	0.47	8.35	2.98	0.67	0
Fe-Mg Diorite	KK-1	55.3	0.8	18.88	9.67	0.14	9.53	5.36	1.71	0.65	0
	KK-2	56.5	0.83	18.12	9.89	0.18	10.03	5.43	1.43	0.71	0
	KK-3	56.6	0.67	17.92	9.37	0.1	9.46	5.51	1.49	0.61	0
	KK-4	55.8	0.71	18.82	9.26	0.12	9.87	5.67	1.42	0.59	0
	KK-5	55.4	0.68	18.3	9.14	0.14	9.52	5.32	1.40	0.58	0
	KK-6	55.2	0.65	18.14	9.23	0.16	9.47	5.42	1.37	0.57	0

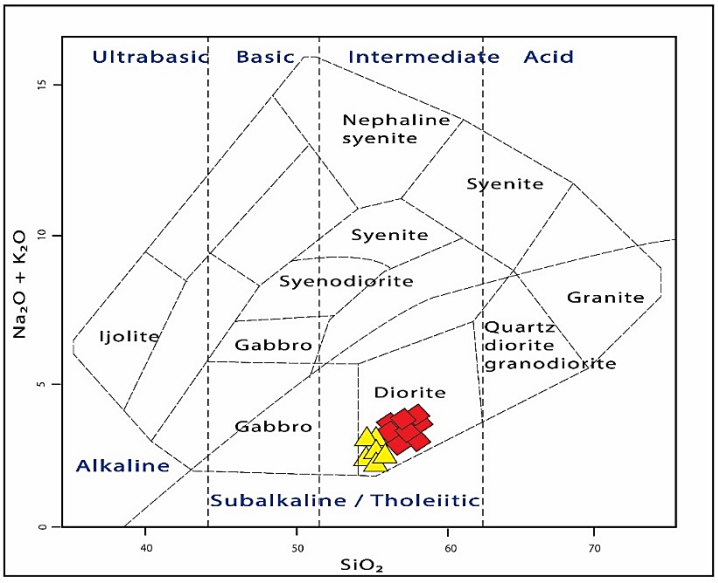

Fig. 5 The total Alkali silica diagram for plutonic rocks (SiO_2 vs Na_2O+K_2O) (Cox et al., 1979).

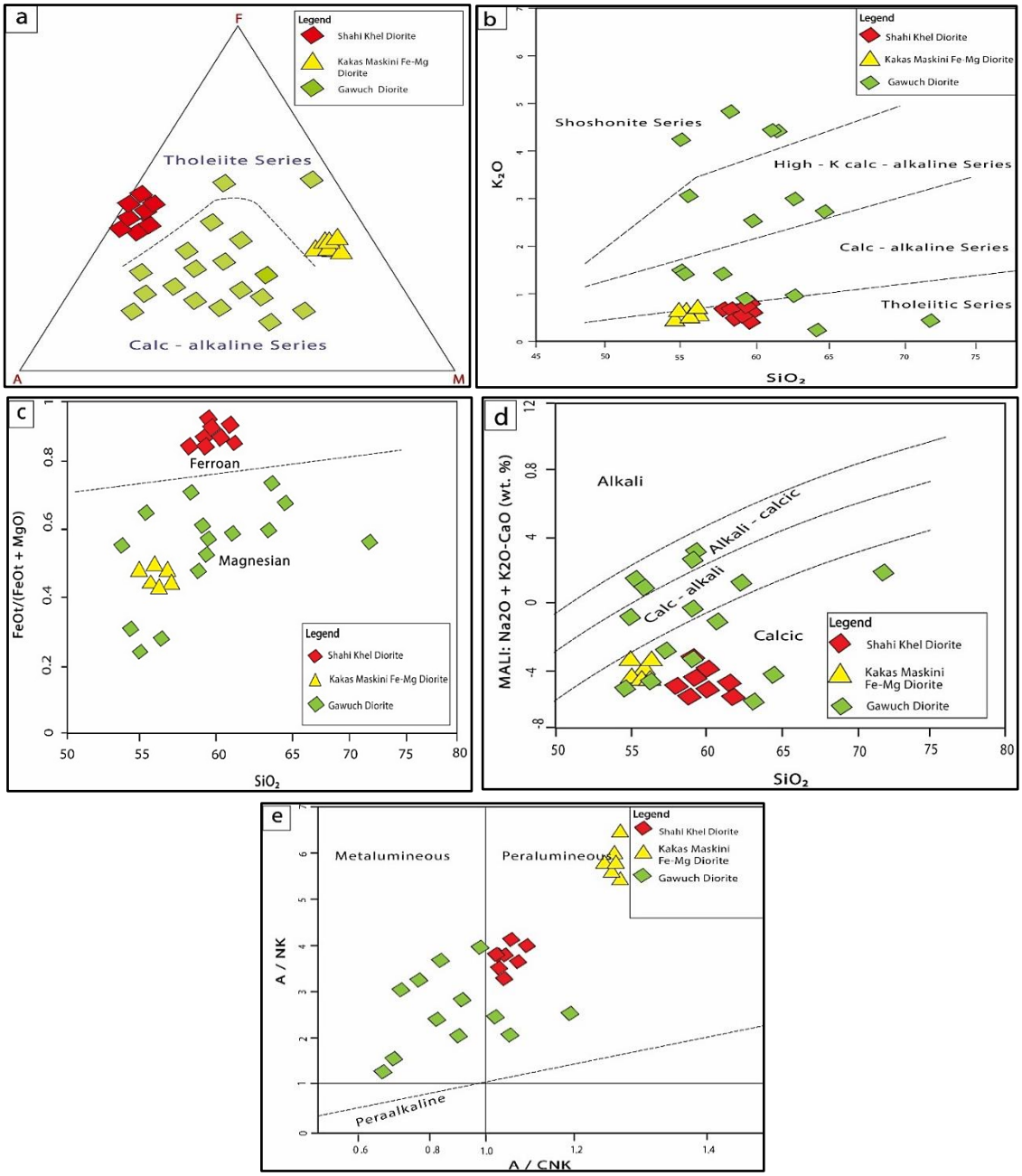

Fig. 6 Petrogenetic series discrimination plots (**a**) AFM plot (Irvine and Barager, 1971) (**b**) SiO_2 vs K_2O plot (Peccerilo and Taylor, 1976) (**c**) Ferron and Magnesian plot (Frost and Frost, 2008; Frost et al., 2001) (**d**) SiO_2 vs modified alkaline lime index (MALI) plot (Frost and Frost, 2008; Frost et al., 2001) (**e**) A/CNK vs A/NK plot of alkalinity series discrimination (Shand, 1943). (Note: The Gawuch Diorite investigated by Tahirkheli et al. (2012) has been used for comparsion throughout this work as that is the only examined diorite section exposed in the vacinity of the Kamila Amphiobolite Belt).

4.2.3. SERIES DISCRIMINATION DIAGRAMS

The series discrimination diagrams are used to classify the igneous rocks based on their chemical composition and chemical characteristics. The AFM plot (Irvine and Barager, 1971) suggests tholeiitic magma series for the Shahi Khel Diorite and Kakas Maskini Fe-Mg Diorite, while suggesting calc-alkaline nature for the Gawuch Diorite (Tahirkheli et al., 2012) (Fig. 6a).

The SiO_2 vs K_2O plot (Peccerillo and Taylor, 1976) shows the magma nature in terms of K_2O concentration. The samples of Shahi Khel Diorite and Kakas Maskini Fe-Mg Diorite fall in the tholeiitic magma while the Gawuch Diorite three samples in the tholeiitic magma series, five samples in the calc-alkaline series, four in high K calc-alkaline series, and four in shoshonite series (Fig. 6b). The tectonic discrimination diagrams FeOt vs FeOt+MgO (Frost and Frost, 2008; Frost et al., 2001) suggest magnesium nature for Kakas Maskini Fe-Mg Diorite and Gawuch Diorite, while, the ferron nature for Shahi Khel Diorite (Fig. 6c). The tectonic discrimination series based on SiO_2 and the modified alkaline lime index (MALI) of (Frost and Frost, 2008; Frost et al., 2001) suggests the

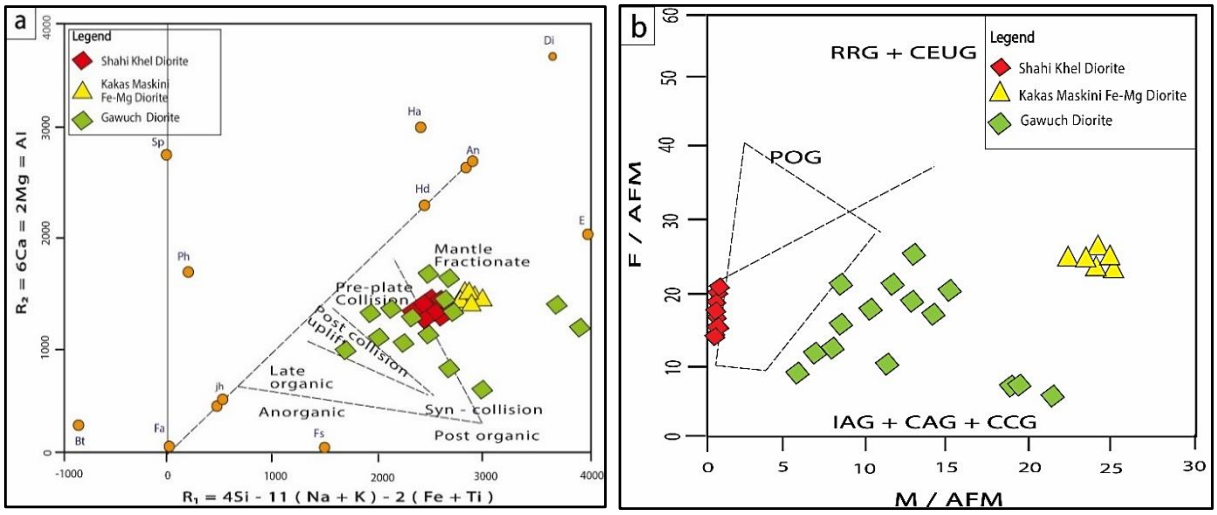

Fig. 7 Tectonic discrimination plot series (**a**)R1-R2 plot (Batchelor and Bowden, 1985) **(b)** M/ AFM vs F/AFM (Maniar and Piccoli, 1989).

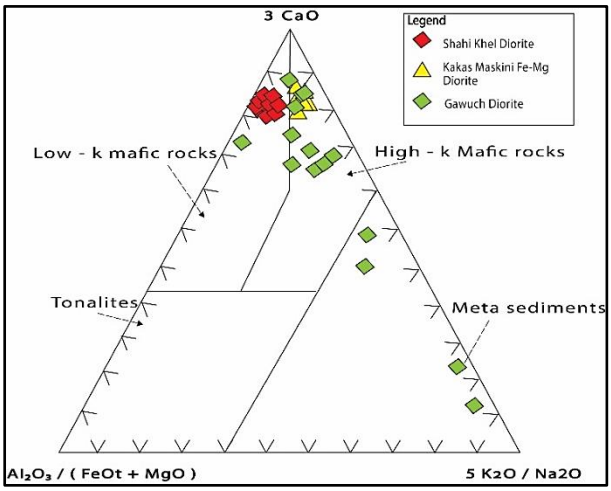

Fig. 8 Magma source discrimination diagrams (Laurent et al., 2014).

calcic nature of Shahi Khel Diorite and Kakas Maskini Fe-Mg Diorite. The Gawuch Diorite eight samples fell in the calcic region, three samples in the calc-alkali portion, and four in alkali calcic nature (Fig. 6d).

4.2.4. ALKALINITY SERIES DISCRIMINATION DIAGRAM

The Molar Al_2O_3-Na_2O-K_2O and A/CNK vs A/NK of Shand (1943) suggest that the representative samples of diorite fall in the peraluminous and metaluminous geochemical boundary (Fig. 6e).

4.2.5. TECTONIC DISCRIMINATION SERIES

The geochemical characteristics of the rocks are linked with specific tectonic settings, and these associations can be understood with the help of tectonic discrimination diagrams for the geochemical signatures of the rocks (Ueki et al., 2018). For instance, the R1-R2 (R1= 4Si-11(Na+K)-2(Fe+Ti), R2 = 6Ca+2Mg+Al) tectonic discrimination diagrams of Batchelor and Bowden (1985) divide these diorites into pre-plate collision, post-collision uplift, and mantle fractionation. The geochemical signatures of the representative samples of the Shah Khel Diorite and Kakas Maskini Fe-Mg Diorite fall in the mantle fractionates fields. The Gawuch Diorite seven samples fall in the mantle fractionates seven in pre plate-collision and one in post-collisional uplift (Fig. 7a). The most complete tectonic classification for the selected samples of Samar Bagh Complex is the M/AFM vs F/AFM plot (Maniar and Piccoli, 1989) shows the Island Arc, Continental Arc, Continental Collision and Post Orogenic Granite (IAG+CAG+ CCG) granitoid nature (Fig. 7b).

4.2.6. SOURCE DISCRIMINATION DIAGRAM

The source discrimination diagram of Laurent et al. (2014) show the fields from which the melts of the rocks are potentially derived. The source diagram suggest a high potassium mafic magma source for the Kakas Maskini Fe-Mg Diorite, low potassium mafic magma source for the Shahi Khel Diorite, and the majority samples of Gawuch Diorite fall in the high potassium mafic rocks (Fig. 8).

4.2.7. HARKER VARIATION DIAGRAMS

Harker variation diagrams are binary plots of major oxides and silicon dioxide, used to get insights into the magma differentiation process (Harker, 1909). The Harker diagrams show the regression analysis of SiO_2 and different major oxides. The regression analysis means the effect of SiO_2 concentrations on the major oxides of the rocks (Yanez et al., 2024; Yang et al., 2019). The SiO_2 vs Al_2O_3 shows a positive trend line for Shahi Khel Diorite, and Kakas Maskini Fe-Mg Diorite. The SiO_2 vs TiO_2 and SiO_2 vs MgO show a negative trend. The SiO_2 vs Na_2O, SiO_2 vs CaO and SiO_2 vs K_2O show a positive trend line for the Shahi Khel Diorite and Kakas Maskini Fe-Mg Diorite as illustrated in Figures 9 a-9e.

5. DISCUSSION

5.1. PETROGRAPHIC IMPLICATIONS

The dominance of plagioclase (up to 87 % in Shahi Khel Diorite and 80 % in Kakas Maskini Fe-Mg Diorite) reflects a mantle-derived magma source that underwent fractional crystallization (Koizumi et al., 2016). The presence of clinopyroxene, amphibole, and magnetite supports a subduction-related setting, where mafic to intermediate magmas evolve through crystallization under moderate pressure (Liu et al., 2024). The sericitization of plagioclase in the Fe-Mg Diorite suggests hydrothermal alteration associated with post-magmatic fluid activity (Bozkaya et al., 2019). The observed patterns of magnetite in association with hornblende indicate prolonged cooling for mineral crystallization (Wen et al., 2017). These petrographic features are consistent with an island arc environment.

5.2. GEOCHEMICAL IMPLICATIONS

The geochemical data reveal that both diorites belong to the tholeiitic magma series and are calc-alkaline to the calcic nature for Gawuch Diorite indicated by the AFM plot. This differentiation of magma generation is controlled by the Fe_2O_3 concentration, which is higher in the Shahi Khel Diorite and Kakas Maskini Fe-Mg Diorite while lower its concentration as compared to Na_2O+K_2O of Gawuch Diorite (Fig. 6a). This data suggests that the magma was generated in subduction zones environments where mantle wedge processes dominate.

The Peccerillo and Taylor plot shows the tholeiitic magma series for both diorites while, the dissimenated nature of Gawuch Diorite because of its variability in K_2O content (Fig. 6b). The lower K_2O values (≤ 1) classify these diorites as low-K tholeiitic rocks, typically of early stage subduction-related magmatism (Zhang et al., 2017).

The FeOt vs FeOt+MgO diagram classifies these diorites into ferron and magnesian nature. (Fig. 6c). The high Fe_2O_3 content in the Fe-Mg diorite reflects its ferron nature, while the Shahi Khel Diorite shows magnesian nature, suggesting differences in their crystallization processes and mantle source composition (Perumalsamy et al., 2024).

The SiO_2 vs MALI plot shows the calcic nature for both diorites while the Gawuch Diorite eight samples fell in calcic due to a higher concentration of CaO as compared to Na_2O, three samples fell in the calc-alkaline portion and four in alkali calcic due to subsequent decreases in CaO as compared to Na_2O and K_2O (Fig. 6d). The Shahi Khel Diorite, Kakas Maskini Fe-Mg Diorite show that the concentration of calcium is greater than the sodium and potassium, thus they are in the range of calcic nature. This classification scheme shows that as sodium and potassium decreases and the subsequent calcium oxide concentration increases, they establish a trend from alkaline to calcic nature (Fig. 6d).

The alkalinity series discrimination diagrams show the aluminum saturation index (ASI) of the igneous rocks. The concentration of aluminum oxide in response to the sodium oxide, potassium oxide, and calcium oxides categorizes the rocks in the alkalinity series discrimination diagrams (du Bray et al., 2019). If the $Al_2O_3 > (CaO+Na_2O+K_2O)$ the rock is considered to be peraluminous. If the $Al_2O_3 < (CaO+Na_2O+K_2O)$ but $Al_2O_3 > (Na_2O+K_2O)$ the rocks are considered to be metaluminous. If the $Al_2O_3 < (Na_2O+K_2O)$ the rocks are considered to be peralkaline (Jung and Pfander, 2007). The Alkalinity series plot of Shand (1943) suggests the peraluminous and metaluminous traits of these diorites (Fig. 6e). The peraluminous and metaluminous nature of Shahi Khel Diorite and Kakas Maskini Fe-Mg Diorite indicates subduction-related tectonic environment where mantle-derived magmas interacted with crustal components during evolution (Nouri et al., 2018). These geochemical signatures align with the prescribed tectonic model involving the intraoceanic subduction of the Neo-Tethys beneath the Paleo-Tethys (Fig. 10).

The source discrimination diagram for Shahi Khel Diorite shows characteristics of low-potassium mafic rocks indicating a mantle source with less crustal contamination (Babazadeh et al., 2024) as shown in Figure 8. This reflects a typical early stage subduction related magma processes, where the mantle wedge undergoes partial melting without significant crustal interaction (Zheng et al., 2020; Alshehri, 2025). The Kakas Maskini Fe-Mg Diorite and Gawuch Diorite are characterized as high-potassium rocks, implying a mantle source enriched in potassium, suggesting a more evolved magma system indicating crustal contamination during ongoing subduction (Abbasi et al., 2024).

The Harker variation diagrams for SiO_2 vs TiO_2 show negative trend line and suggest the formation of more silica saturated rocks and consumption of TiO_2 increases in the crystallization of titanium bearing minerals in the magmatic differentiation process (Fig. 9a). This negative relationship is consistent with the tholeiitic nature and characterisitc of subduction

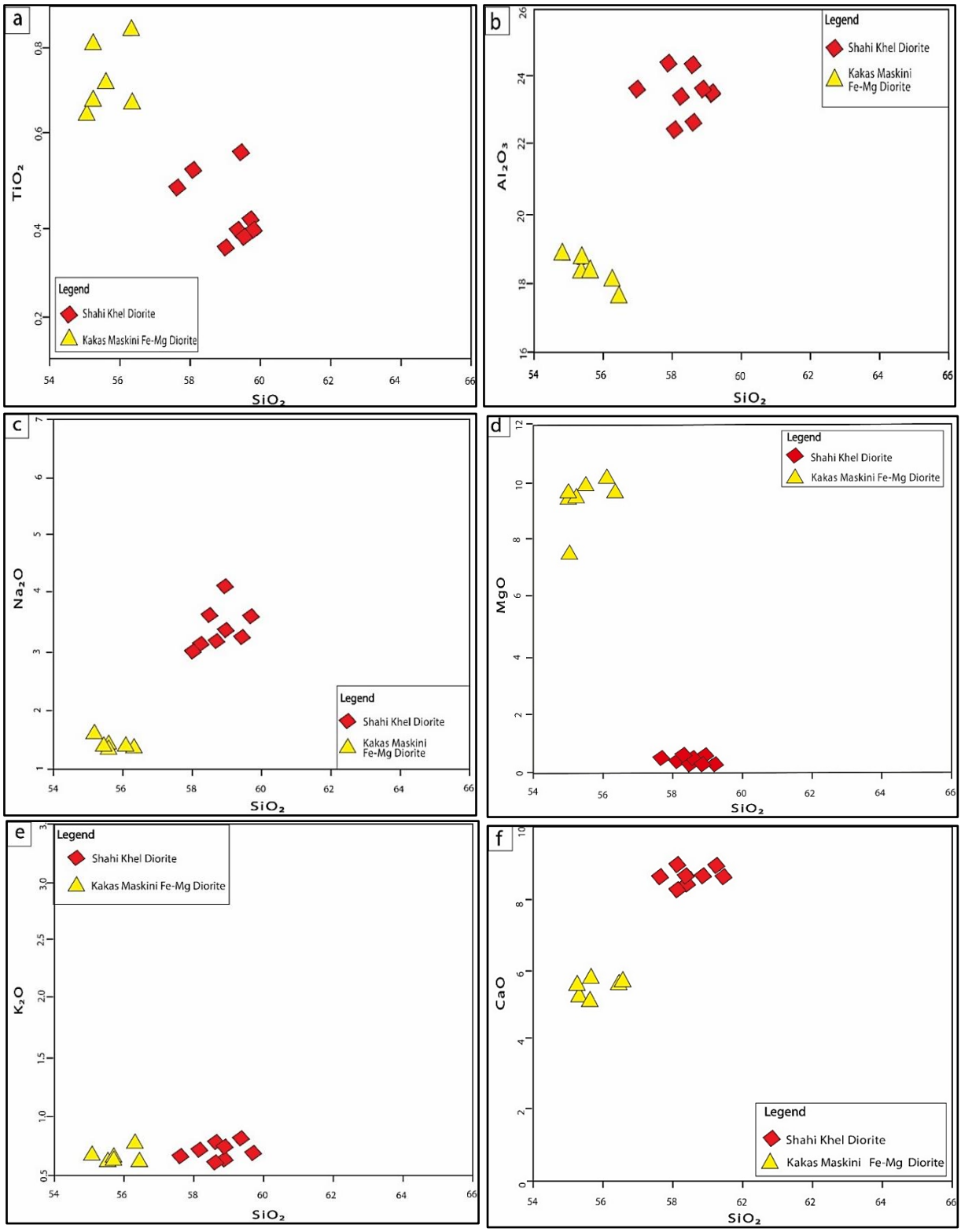

Fig. 9 Harker variations plots for diorite and Fe-Mg diorite (**a**) SiO_2 vs TiO_2, (**b**) SiO_2 vs Al_2O_3, (**c**) SiO_2 vs Na_2O, (**d**) SiO_2 vs MgO, (**e**) SiO_2 vs K_2O (**f**) SiO_2 vs CaO.

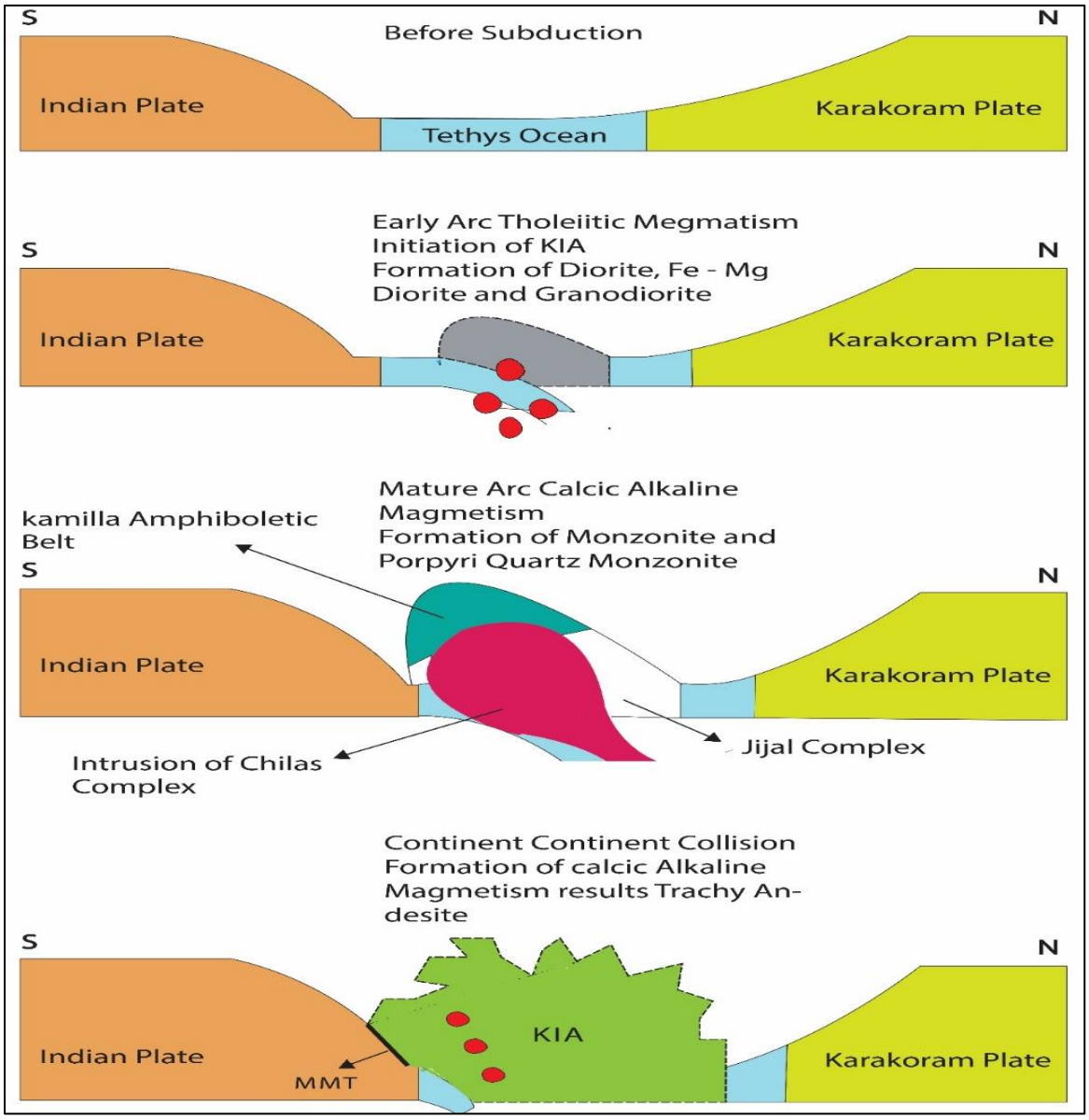

Fig. 10 A schematic model showing various stages of magma evaluation of KIA and formation of Samar Bagh Complex rocks modified after Shah and Shervais (1999; Khan et al. (1993).

related magmas where fractional crystallization and magma evolution occur at moderate pressure, leading to the depletion of titianum in the evolved melts (Abdelfadil et al., 2022).

The Shahi Khel Diorite shows slightly higher SiO_2 and Al_2O_3 as compared to the Kakas Maskini Fe-Mg Diorite, indicating a more evolved nature. The SiO_2 vs Al_2O_3 shows a positive trend line for Shahi Khel Diorite, Kakas Maskini Fe-Mg Diorite (Fig. 9b). This relationship reflects the crystallization of pyroxenes and amphibole and the subsequent enrichment of aluminum in the remaining magma (Dias, 2024). This trend suggests that plagioclase is in a dominant crystallizing phase, which contributes to higher Al_2O_3 content in the magma (Yousefi et al., 2024). This positive trend is common in subduction-related magmas, where mantle-derived melts evolve through interaction with crust and fractional crystallization (Berry, 2024).

The SiO_2 vs Na_2O shows a positive trend line for the Shah Khel Diorite and Kakas Maskini Fe-Mg Diorite. This positive relationship reflects the crystallization of early formed pyroxenes and amphiboles that are low in Na_2O, leaving the residual melt enriched in sodium (Bailey and Schairer, 1966). The trend supports subduction-related settings where fractional crystallization and melt evolution lead to sodium enrichment in more evolved magmas (Fig. 9c).

The SiO_2 vs MgO binary plots show the opposite correlation for diorite and Fe-Mg Diorite. The negative trend reflects the removal of mafic minerals during the early stage of magma cooling (Fig. 9d). This trend is associated with mantle wedge magmas evolving through fractional crystallization

Table 3 Comparative Analysis of the Shahi Khel, Kakas Maskini and Gawuch Diorite on various Discrimination series.

Discrimination series	Plot Classification series	Rock Type	Results	Discussion
Rock Classification Diagram	SiO_2 Vs Na_2O+ K_2O Classification (Cox et al., 1979)	Shahi Khel Diorite Kakas Maskini Fe-Mg Diorite Gawuch Diorite	Diorite rock Diorite rock Diorite rock	Diorite rocks because of SiO_2 > 55 and Na_2O+K_2O>3.
Magmatic Series Discrimination Diagrams	AFM plot (Irvine and Barager, 1971)	Shahi Khel Diorite Kakas Maskini Fe-Mg Diorite Gawuch Diorite	Tholeiitic Series Tholeiitic Series Calcic Alkaline Series	Shahi Khel Diorite and Kakas Maskini Fe-Mg Diorite has higher Fe_2O_3 concentration while lower Na_2O vs K_2O concentration as compared to Gawuch diorite
	SiO_2 vs K_2O plot (Peccerillo and Taylor, 1976)	Shahi Khel Diorite Kakas Maskini Fe-Mg Diorite Gawuch Diorite	Tholeiitic Series Tholeiitic Series Tholeiitic-Shoshonite series	The K_2O percentage of Shahi Khel and Kakas Maskini Fe-Mg Diorite are comparatively low ($K_2O \leq 1$) than the Gawuch Diorite. The Gawuch Diorite has irregular concentration of K_2O, so their samples fill all boundaries of the plot.
	SiO_2 vs FeOt/(FeOt+MgO plot (Frost and Frost, 2008; Frost et al., 2001)	Shahi Khel Diorite Kakas Maskini Fe-Mg Diorite Gawuch Diorite	Ferron Magnesian Magnesian	The Shahi Khel Diorite has low MgO concentration than the Kakas Maskini Fe-Mg Diorite and Gawuch diorite
Alkalinity Series Discrimination Diagrams	Molar Al_2O_3-Na_2O-K_2O plot*[1]	Shahi Khel Diorite Kakas Maskini Fe-Mg Diorite Gawuch Diorite	Peraluminous Metaluminous Peraluminous Metaluminous Peraluminous Metaluminous	Diorite rock falls in the Peraluminous to Metaluminous because of Higher concentration of Al_2O_3.
	A/CNK vs A/NK plot (Shand et al., 1943	Shahi Khel Diorite Kakas Maskini Fe-Mg Diorite Gawuch Diorite	Perluminous Perluminous Metaluminous	The Shahi Khel Diorite and Kakas Maskini Fe-Mg Diorite has A/CNK value > 1.0 thus they show Peraluminous while the Gawuch dioirite has A/CNK <1.0 they show Metaluminous
	B-A plot* (Villaseca et al., 1998)	Shahi Khel Diorite Kakas Maskini Fe-Mg Diorite Gawuch Diorite	Mederately Peraluminous Mederately Peraluminous Peraluminous - Metaluminous	The Shahi Khel Diorite and Fe-Mg Diorite has intermediate value of A=Al-(K+Na+2Ca) thus they are Moderately peraluminous while the Gawuch Diorite majority of samples having A value less than 0 % show metaluminous while some samples have high value show moderately to high peraluminous nature
	B-A plot* (Debon and Le Fort, 1983)	Shahi Khel Diorite Kakas Maskini Fe-Mg Diorite Gawuch Diorite	Peraluminous Peraluminous Peraluminous - Metaluminous	The Shahi Khel Diorite and Fe- Mg Diorite has A=Al-(K+Na+2Ca) value upto 100 show peraluminous while the Gawuch Diorite majority of samples having A value less than 0 % show metaluminous while some samples have value up to 150 suggests peraluminous nature

Tectonic Discrimination Diagrams	R1- R2 plot (Batchelor and Bowden, 1985)	Shahi Khel Diorite	Mantle Fractinoates	The R1-R2 plot the Shahi Khel Diorite and Fe-Mg Diorite have more value of R1≥ 3000 suggesting mantle fracionates field while some of the gawuch diorite has valueof 3000 showing Mantle fractionates and some have less than 3000 suggesting pre-plate collision zone
		Kakas Maskini Fe-Mg Diorite	Mantle Fractinoates	
		Gawuch Diorite	Mantle Fractinoates-Pre-plate collision	
	M/AFM vs F/AFM (Maniar and Piccoli, 1989)	Shahi Khel Diorite	IAG+CAG+CCG	**T**he Shahi Khel Diorite Kakas Maskini Fe-Mg Diorite and Gawuch Diorite M/AFM value or not with in the range of 1-5 agains the F/AFM value of 10-20
		Kakas Maskini Fe-Mg Diorite	IAG+CAG+CCG	
		Gawuch Diorite	IAG+CAG+CCG	
Source Discrimination Diagrams	Magma Source Discrimination Plot (Laurent et al., 2004)	Shahi Khel Diorite	Low K Mafic rocks	The Shahi Khel Diorite has more Cao Al_2O_3/(FeOt+MgO) concnetration than the Kakas Maskini Fe-Mg Diorite and Gawuch Diorite which have higher value of Cao and K_2O/Na_2O
		Kakas Maskini Fe-Mg Diorite	High K Mafic rocks	
		Gawuch Diorite	High K Mafic rocks	

[1] The asterick plots (*) were not included in the results sections they provide similar trends and interpretations to the included corresponding discrimination diagram,ensuring conciseness and avoiding redundancy in the manuscript.

(Parra-Encalada et al., 2024). The negative plot also supports the tholeiitic nature of magma as declining of MgO occurs. The SiO_2 vs K_2O shows a positive relationship with each other for the diorite and Fe-Mg diorite (Fig. 9e). This positive trend suggests the incompatibility of potassium bearing minerals in early crystallizing magma (Mbassa et al., 2020).

The SiO_2 vs CaO show a positive relationship for Shah Khel Diorite and Kakas Maskini Fe-Mg Diorite (Fig. 9f). This trend reflects that these diorites are products of magma differentiation under moderate pressure, where calcium bearing minerals crystallized (El-Desoky and Hafez, 2018).

5.3. TECTONIC IMPLICATIONS AND TECTONIC MODEL

The tectonic discrimination diagrams place both diorite types in the mantle fractionates field, supporting their origin from subduction related processes. The M/AFM vs F/AFM plot further classifies them as island arc granitoids (IAG) with contributions from the continental arc and collision related processes. The petrographic and geochemical data, along with discrimination diagrams, reconstruct the tectonic model for the Samar Bagh Complex. The overall data suggest that the Shahi Khel Diorite and Kakas Maskini Fe-Mg Diorite are part of Kamila Amphibolite Belt and represent the rocks of lower to intermediate island arc crust, followed by the continental arc and collisional arc rocks (Ahmad et al., 2013). These rocks are uplifted and exposed as a result of late Cretaceous imbrication and folding of the Kohistan-Karakorum collision at Main Korakorum Thrust (MKT) or obduction of the Indian Plate along MMT (Pecher et al., 2008). The Kamila Amphibolite Belt was a metamorphosed oceanic basement invaded by the subduction of the Jijal and Chilas Complexes (Searle and Taylor, 2010). The multiphase magma nature and multi-stage collisional history of the Kamila Amphibolite Belt show the various tectonic events of magma generation in the intraoceanic period of KIA (Petterson, 2019). The early intraoceanic subduction of the Neo-Tethys beneath the Paleo-Tethys, with mantle wedge melting generated tholeiitic magmas (Fu et al., 2024). The magmas intruded the arc crust, forming diorites with low-K, ferron, and magnesian characteristics. The continued subduction and mantle fractionate led to the differentiation of mantle derived magmas, forming the Shahi Khel and Kakas Maskini Fe-Mg Diorite (Wang et al., 2020). The hydrothermal alteration (sericitized plagioclase) and the presence of epidote veins in Kakas Maskini Fe-Mg Diorite reflect post-magmatic processes linked to crustal uplift and fluid circulation during the collision of the KIA with the Indian Plate (Rothstein, 1997). As the subductions proceed, the intrusion of Chilas Complex, the intra arc rifting initiates which produce the calc-alkaline magmas generation results in the porphyry quartz monzonite, and monzonite which are related to continental arc granites and uplifted in the post collisions of the Karakorum and KIA (Heuberger, 2004). The volcanic rocks of the Samar Bagh Complex show the calc-alkaline nature of magma and formed as a result of Continent-Continent Collision (Late Orogenic) (Singh et al., 2023) (Fig. 10). The Gawuch Diorites are exposed at Chitral located at the northwestern margin of KIA. This diorite belt is part of the Lowari Pluton of the Kohistan Batholith (Tahirkheli et al., 2012). The suggested tectonic model for Gawuch Diorite is pre-plate collision and island arc related formed during subduction of the Neo-Tethys beneath the Paleo-Tethys and Karakorum Plate.

6. CONCLUSION

The study examined the diorite and Fe-Mg diorite of the Samar Bagh Complex, revealing key insights into petrographic and geochemical characteristics. These intermediate rocks are primarily composed of plagioclase, clinopyroxene, amphiboles, and biotite and were identified as a product of tholeiitic magma series with paraluminous to metaluminous nature signifying a dual contribution from mantle and crustal sources. These findings highlight the role of subduction zone magmatism in shaping the geochemical characteristics of the diorites. Geochemical discrimination series suggest these rocks were formed through mantle fractionation during the subduction of the Neo-Tethys ocean beneath the Paleo-Tethys ocean. In short, the integration of petrographic observation geochemistry and tectonic study confirms that these diorites were formed through fractional crystallization and evolving under subduction-related tectonics processes. These findings contribute to the understanding of petrogenetic and geochemical patterns of intermediate rocks in the Kamila Amphibolite Belt and provide a framework for future exploration of their economic potential in mineralization and construction materials.

ACKNOWLEDGMENTS

The authors extend their appreciation to Abdullah Alrushaid Chair for Earth Science Remote Sensing Research at King Saud University for funding

CONFLICTS OF INTEREST

The authors declare no conflicts of interest.

REFRENCES

Abbasi, S., Tabatabaei Manesh, S.M., Karimi, S. and Parfenova, O.V.: 2014, Relative contributions of crust and mantle to generation of Oligo-Miocene medium-K calc-alkaline I-type granitoids in a subduction setting-a case study from the Nabar Pluton, central Iran. Petrology, 22, 310−328. DOI: 10.1134/S0869591114030023

Abdelfadil, K.M., Saleh, G.M., Putiš, M. and Sami, M: 2022, Mantle source characteristics of the late Neoproterozoic post-collisional gabbroic intrusion of Wadi Abu Hadieda, north Arabian-Nubian Shield, Egypt. Jour of Afri Earth Sci, 194, 104607 DOI: 10.1016/j.jafrearsci.2022.104607.

Ahmad, I., Jan, M.Q. and Di Petro J.A.: 2003, Age and tectonics implications of granitoid rocks from the Indian plate of Northern Pakistan. Jour. Virt. Explorer, 11, 21−28.

Ahmed Khan, M., Rehman, S.U., Mehmood, K., Asif Khan, M. and Ahsan, N.: 2013, Geochemical characterization and petrogenesis of Niat-Jal amphibolites, southeast Kohistan, Pakistan. Iran J. Sci. Technol. Trans. A, Sci., 37, 2, 147−159.

Ali, A., Ahmad, S., Ahmad, S., Khan, M.A., Khan, M.I. and Rehman, G.: 2021, Tectonic Framework of Northern Pakistan from Himalaya to Karakoram. Struc. Geol. and Tect. Field Guidebook, 1, 367−412. DOI: 10.1007/978-3-030-60143-0_12

Ali, M., Zhao, K.D., Wang, C., Rehman, H. U., Hussain, A., Mahar, M.A. and Lutfi, W.: 2024, Geochemical and isotopic constraints on the origin and evolution of the Matum-Das tonalite and mafic enclaves from the Kohistan Batholith, Northern Pakistan. Lithos, 107535. DOI: 10.1016/j.lithos.2024.107535

Alshehri, F., Shahab, M., Azer, M.K. et al.: 2025, An integrated remote sensing and geochemical approach for mapping the Kamal layered mafic intrusion in the Arabian Shield, Northwest Saudi Arabia. Environ. Earth Sci., 84, 40. DOI: 10.1007/s12665-024-11995-3

Babazadeh, S., Furman, T., Santosh, M., Raeisi, D., Choi, S.H. and D'Antonio, M.: 2024, Middle to Late Miocene K-rich magmatism in Central Iran: Geochemical characterization of the post-collision mantle beneath the Urumieh–Dokhtar magmatic arc. Chemical Geology, 665, 122308. DOI: 10.1016/j.chemgeo.2024.122308

Bailey, D.K. and Schairer, J.F.: 1966, The System Na_2O – Al_2O_3 – Fc_2O_3 – SiO_2 at 1 Atmosphere, and the Petrogenesis of Alkaline Rocks. Jour of Petrol, 7(1), 114−170. DOI: 10.1093/petrology/7.1.114

Batchelor, R.A. and Bowden, P.: 1985, Petrogenetic interpretation of granitoid rock series using multicationic parameters. Chem. Geol., 48(1-4), 43−55. DOI: 10.1016/0009-2541(85)90034-8

Berry, J.: 2024, An integrated accessory mineral approach to understanding postsubduction magmas and mineralisation. Doctoral dissertation, University of Leicester.

Bozkaya, Ö., Bozkaya, G., Yılmaz, H., Hozatlıoğlu, D. and Banks, D.A.: 2019. The origin, age and duration of hydrothermal alteration associated with iron skarn mineralization determined from clay/phyllosilicate minerals, Bizmişen-Erzincan, East-Central Turkey. Ore Geology Reviews, 115, 103179. DOI: 10.1016/j.oregeorev.2019.103179

Cox, K.G., Bell, J.D. and Pankhurst, R.J.: 1979, The interpretation of igneous rocks. Allen and Unwin London, 450. DOI: 10.1007/978-94-017-3373-1

Debon, F. and Le Fort, P.: 1983, A chemical–mineralogical classification of common plutonic rocks and associations. Ear. and Envir. Sci. Trans. of the Royal Soc. of Edin., 73(3), 135−149. DOI: 10.1017/S0263593300010117

Dias, A.: 2024, Relationship between dioritic magmatism and oxide ore forming processes in the Beja Igneous Complex, Portugal. Doctoral dissertation.

du Bray, E.A., John, D., Colgan, J., Vikre, P.G., Cosca, M.A. and Morgan, L.E.: 2019, Petrology of volcanic rocks associated with silver-gold (Ag-Au) epithermal deposits in the Tonopah, Divide, and Goldfield Mining Districts, Nevada, US Geol. Sur., 2019−5024. DOI: 10.3133/sir20195024

El-Desoky, H.M. and Hafez, H.M.: 2018, Petrology, Geochemistry and Mineralogy of the Hydrothermally Altered Rock Units at Wadi Dara, North Eastern Desert, Egypt. Ann. Geol. Surv. Egypt, 35, 103−140.

Frost, B.R. and Frost, C.D.: 2008, A geochemical classification for feldspathic igneous rocks. Journal of Petrology, 2008, 49(11), 1955−1969. DOI: 10.1093/petrology/egn054

Frost, B.R., Barnes, C.G., Collins, W.J., Arculus, R.J., Ellis, D.J. and Frost, C.D.: 2001, A geochemical classification for granitic rocks. Journal of Petrology, 42(11), 2033−2048. DOI: 10.1093/petrology/42.11.2033

Fu, C., Yan, Z., Aitchison, J.C., Xiao, W., Buckman, S. and Wang, B.: 2024, Subduction within the Proto-Tethys Ocean revealed by recognition of the earliest Phanerozoic intra-oceanic arc, northern Tibetan Plateau. Earth and Sp Sci, 11(3). DOI: 10.1029/2023EA002985

Gibbons, A.D., Zahirovic, S., Müller, R.D., Whittaker, J.M. and Yatheesh, V.: 2015, A tectonic model reconciling evidence for the collisions between India, Eurasia and intra-oceanic arcs of the central-eastern Tethys. Gondwana Research, 28(2), 451−492. DOI: 10.1016/j.gr.2015.01.001

Harker, A.: 1909, The natural history of igneous rocks. Macmillam, New York, Methuen and Co., London, 344 pp.

Heuberger, S.: 2004, Kinematics of the Karakoram-Kohistan suture zone, chitral, NW Pakistan. Doctoral dissertation, ETH Zurich.

Irvine, T.N. and Baragar, W.R.A.F.: 1971, A guide to the chemical classification of the common volcanic rocks. Canad. Jour. of Ear. Sci, 8(5), 523−548. DOI: 10.1139/e71-055

Jan, M.Q.:1990, Geochemistry of amphibolites from the southern part of the Kohistan arc, N.Pakistan. Mineralogical Magazine, 52(365). DOI: 10.1180/minmag.1988.052.365.02

Jung, S. and Pfander, J.A.: 2007, Source composition and melting temperatures of orogenic granitoids: constraints from CaO/Na2O, Al2O3/TiO2 and accessory mineral saturation thermometry. Europ. Jourl of Miner., 19(6), 859. DOI: 10.1127/0935-1221/2007/0019-1774

Kakar, S.K., Badshah, M.S. and Khan, J.: 1973, The geology of the Jandul valley, Western Dir. Geoll Bull. Uni.of Pesh, 6, 54−73.

Khaliq, A.: 1991, Primary geochemistry and secondary dispersion from gold prospects in Karakoram and Hindu Kush, northern Pakistan. University of Leicester, United Kingdom.

Khan, M.A., Jan, M.Q. and Weaver, B.L.: 1993, Evolution of the lower arc crust in Kohistan, N. Pakistan: temporal arc magmatism through early, mature and intra-arc rift stages. Geol. Soc., Lond, SP 74(1), 123−138. DOI: 10.1144/GSL.SP.1993.074.01.10

Khan, M.A., Rehman, S. and Ahsan, N.: 2012, Geology and geochemistry of Sumal amphibolites, Kamila amphibolite unit, southeast Kohistan, Pakistan. Int. J. Agric. Appl. Sci, 4(2).

Khan, M.A., Stern, R.J., Gribble, R.F. and Windley, B.F.: 1997, Geochemical and isotopic constraints on subduction polarity, magma sources, and palaeogeography of the Kohistan intra-oceanic arc, northern Pakistan Himalaya. Jour. of the Geol. Soc., 154(6), 935−946. DOI: 10.1144/gsjgs.154.6.0935

Koizumi, N., Okudaira, T. and Ogawa, D.: 2016, Geochemical characteristics of hydrous basaltic magmas due to assimilation and fractional crystallization: the Ikoma gabbroic complex, southwest Japan. Miner. & Petrol., 110, 639–662. DOI: 10.1007/s00710-016-0423-9

Laurent, O., Martin, H., Moyen, J.F. and Doucelance, R.: 2014, The diversity and evolution of late-Archean granitoids: Evidence for the onset of “modern-style” plate tectonics between 3.0 and 2.5 Ga. Lithos, 205, 208−235. DOI: 10.1016/j.lithos.2014.06.012

Le Maitre, R.W.: 2002, Igneous rock: a classification and glossary of terms. 2nd Edition, Cambridge University Press.

Luo, C.H., Wang, R., Nebel, O. and Li, Q.W.: 2024, Amphibole fractionation as a key driver for oxidation of magmas in convergent margins. Earth & Pl Sci Lett, 641, 118851. DOI: 10.1016/j.epsl.2024.118851

Majid, M. and Paracha, F.A.: 1980, Calc-alkaline magmatism at destructive plate margin in Kohistan, northern Pakistan. Geol. Bull. Univ. Peshawar,13, 109−120.

Majid, M., Shah, M. T., Latif, A., Aurangzeb. and Kamal, M.: 1989, Major element abundance in the Kalam Lauas. Geol. Bull. Univ. Peshawar,14, 45−62.

Maniar, P.D. and Piccoli, P.M.: 1989, Tectonic discrimination of granitoids. Geol. Soci. of Amer. Bull., 101(5), 635−643. DOI: 10.1130/0016-7606(1989)101

Mbassa, B.J., Njonfang, E., Ngwa, C.N., Grégoire, M., Itiga, Z., Kamgang, P. and Mbossi, E.F.: 2020, Mineral chemistry and descriptive petrology of the Pan-African high-K granitoids and associated mafic rocks from Mbengwi, NW Cameroon: petrogenetic constraints and geodynamic setting. Jour of Geosci and Geomat, 8(2), 58−75. DOI: 10.12691/jgg-8-2-2

Nakazawa, C., Rehman, H.U., Yamamoto, H. and Zafar, T.: 2020, Zirconium in rutile thermometry from garnet granulites of the Jijal complex of Kohistan arc, NW Himalaya. J Miner Petrol Sci, 115(2), 152−161. DOI: 10.2465/jmps.191226

Nouri, F., Azizi, H., Stern, R. J., Asahara, Y., Khodaparast, S., Madanipour, S. and Yamamoto, K.: 2018, Zircon U-Pb dating, geochemistry and evolution of the Late Eocene Saveh magmatic complex, central Iran: Partial melts of sub-continental lithospheric mantle and magmatic differentiation. Lithos, 314, 274-292. DOI: 10.1016/j.lithos.2018.06.013

Parra-Encalada, D., Larrea, P., Loaiza, C., Cartagena, R., Salinas, S., Godoy, B. and Le Roux, P.: 2024, Decoding subcontinental lithosphere processes: The key role of fractional crystallization in Central Andes monogenetic volcanism-Insight from El Negrillar volcanic field, Chile. Lithos, 464, 107427. DOI: 10.1016/j.lithos.2023.107427

Peccerillo, A., and Taylor, S. R.: 1976, Geochemistry of Eocene calc-alkaline volcanic rocks from the Kastamonu area, northern Turkey. Contr. to miner. and petr., 58, 63-81. DOI: 10.1007/BF00384745

Pecher, A., Seeber, L., Guillot, S., Jouanne, F., Kausar, A., Latif, M. and, Van Melle, J.: 2008, Stress field evolution in the northwest Himalayan syntaxis, northern Pakistan. Tectonics, 27(6). DOI: 10.1029/2007TC002252

Perumalsamy, C., Vijay Anand, S., Nagarajan, R., Mukherjee, B.: 2024, Petrogenesis of S-type Ladakh granite and mafic microgranular enclaves in the southern margin of Ladakh batholith: An evidence of crust–mantle interaction during the collision between Indian and Eurasian plates. Island Arc, 33(1), e12520. DOI: 10.1111/iar.12520

Petterson, M. G., and Windley, B. F.: 1991, Changing source regions of magmas and crustal growth in the Trans-Himalayas: evidence from the Chalt volcanics and Kohistan batholith, Kohistan, northern Pakistan. Ear. and Plan. Sci. Letters, 102(3-4), 326-341. DOI: 10.1016/0012-821X(91)90027-F

Petterson, M.G.: 2010, A review of the geology and tectonics of the KIA, north Pakistan. Geol. Soc., Lond, SP, 338(1), 287−327. DOI: 10.1144/SP338.14

Petterson, M.G.: 2019, The plutonic crust of Kohistan and volcanic crust of Kohistan–Ladakh, north Pakistan/India: lessons learned for deep and shallow arc processes Geol. Soc., Lond, SP, 483(1), 123−164. DOI: 10.1144/SP483.4

Rehman, H. U., Seno, T., Yamamoto, H. and Khan, T.: 2011, Timing of collision of the Kohistan–Ladakh Arc with India and Asia: debate. Island Arc,20(3), 308−328. DOI: 10.1111/j.1440-1738.2011.00774.x

Rehman, H.U., Khan, T., Lee, H.Y., Chung, S.L., Jan, M.Q., Zafar, T. and Murata, M.: 2021, Petrogenetic source and tectonic evolution of the Neoproterozoic Nagar Parkar Igneous Complex granitoids: Evidence from zircon Hf isotope and trace element geochemistry. Precambrian Research, 354. DOI: 10.1016/j.precamres.2020.106047

Rothstein, D. A.: 1997, Metamorphism and denudation of the eastern peninsular ranges batholith, Baja California Norte, Mexico. University of California, Los Angeles.

Sarwar, A.: 1997. Litho and Stream sediments geochemical investigation for base and precious metal in Timergara, Maidan and Jandual area, District Dir, Northern Pakistan. (M.Phil. Thesis). NCEG Peshawar.

Searle, M.P., Khan, M.A., Fraser, J.E., Gough, S.J. and Jan, M.Q.: 1999, The tectonic evolution of the Kohistan-Karakoram collision belt along the Karakoram Highway transect north Pakistan. Tectonics,18(6), 929−949. DOI: 10.1029/1999TC900042

Searle, M.P. and Treloar, P.J.: 2010, Was Late Cretaceous–Paleocene obduction of ophiolite complexes the primary cause of crustal thickening and regional metamorphism in the Pakistan Himalaya? Geol Soci London, SP, 338(1), 345−359. DOI: 10.1144/SP338.16

Shah, M.T. and Shervais, J.W.: 1999, The Dir-Utror metavolcanic sequence, Kohistan arc terrane, northern Pakistan. Jour. of Asi. Ear. Sci., 17(4), 459−475. DOI: 10.1016/S1367-9120(99)00009-7

Shah, M.T., Shervias, J.W. and Ikramuddin, M., 1994, The Dir Meta-volcanic sequence: calcalkaline magmatism in the Kohistan arc terrane, Northern Pakistan. Geol. Bull. Univ. Peshawar, 27, 9−27.

Shahab, M., Ali, L. and Alshehri, F: Integrated remote sensing, petrographic, and mineralogical techniques for mapping of marble deposits in the vicinity of the ophiolite sequence in North Pakistan. Geol. acta, 23. DOI: 10.1344/GeologicaActa2025.23.4

Shand, S.J.: 1943, Eruptive rocks: their genesis, composition, classification, and their relation to ore-deposits with a chapter on meteorite, Wiley, New York.

Singh, N.L., Akhtar, S., Singh, A.K., Singh, B.P., Saikia, A. and Jeelani, S.H.: 2023, Petrogenesis and tectonic implications of the Late Cretaceous to Paleogene calc-alkaline volcanic rocks, Ladakh Himalaya. Jour of Asi Earth Sci, 253, 105700. DOI: 10.1016/j.jseaes.2023.105700

Sullivan, M.A., Windely, B.F., Saaunders, B.F., Hayens, J.R. and Rex, D.C.: 1993, A palaeogeographic reconstruction of the Dir Group: evidence for magmatic arc migration with in Kohistan, N. Pakistan. Geol. Soc. Lond, SP, 74, 139−160. DOI: 10.1144/GSL.SP.1993.074.01.11

Tahirkheli, T., Shah, M.T., Khan, M.A. and Bilqees, R.: 2012, Mineralogy and geochemistry of diorites and associated hydrothermal sulfide mineralization of Gawuch Formation in Drosh area, Chitral, northern Pakistan. Journ. of Him. Ear. Sci, 45(1).

Ueki, K., Hino, H. and Kuwatani, T.: 2018, Geochemical discrimination and characteristics of magmatic tectonic settings: A machine-learning-based approach. Geoche., Geophy., Geosys, 19(4), 1327−1347. DOI: 10.1029/2017gc007401

Villaseca, C., Barbero, L. and Rogers, G.: 1998, Crustal origin of Hercynian peraluminous granitic batholiths of Central Spain: petrological, geochemical and isotopic (Sr, Nd) constraints. Lithos, 43(2), 55−79. DOI: 10.1016/S0024-4937(98)00002-4

Wang, J., Dan, W., Wang, Q. and Tang, G.J.: 2021, High-Mg# adakitic rocks formed by lower-crustal magma differentiation: mineralogical and geochemical evidence from garnet-bearing diorite porphyries in central Tibet. Journal of Petrology, 62(4). DOI: 10.1093/petrology/egaa099

Wen, G., Li, J. W., Hofstra, A.H., Koenig, A.E., Lowers, H.A. and Adams, D.: 2017, Hydrothermal reequilibration of igneous magnetite in altered granitic plutons and its implications for magnetite classification schemes: Insights from the Handan-Xingtai iron district, North China Craton. Geochi et Cosmochi Acta, 213, 255−270. DOI: 10.1016/j.gca.2017.06.043

Yáñez-Dávila, D., Santoyo, E., González-Partida, E., Pandarinath, K., Santos-Raga, G., Mishra, S. and Gómez-Salgado, Z.G.: 2024, Hydrothermal Signatures Discovered in Outcropping Rocks of the Los Humeros Geothermal Field (Mexico): A Geochemometric Exploration Case Study. Geofluids, 2316078. DOI: 10.1155/2024/2316078

Yang, Z.F., Li, J.; Jiang, Q.B., Xu, F., Guo, S.Y., Li, Y. and Zhang, J.: 2019, Using major element logratios to recognize compositional patterns of basalt: Implications for source lithological and compositional heterogeneities. Jour. of Geophy. Reser: Solid Earth, 124(4), 3458−3490. DOI: 10.1029/2018JB016145

Yousefi, F., Lentz, D.R. and Papadopoulou, L.: 2024, Plagioclase-hosted Crystallized Melt Inclusions within Hypabyssal Volcanic Rocks of the Torud-Ahmad Abad Magmatic Belt, Iran: Analysis of Origin and Fractionation Processes. Earth Science Research, 13(1), 1−13. DOI: 10.5539/esr.v13n1p13

Zafar, T., Leng, C.B., Mahar, M.A., Alam, M., Zhang, X.C., Chen, W.T. and Rehman, S.U.: 2020b, Petrogenesis, platinum-group element geochemistry and geodynamic evolution of the Cretaceous Chilas gabbros, Kohistan island arc, NE Pakistan. Lithos, 372, 105691. DOI: 10.1016/j.lithos.2020.105691

Zafar, T., Leng, C.B., Mahar, M.A., Rehman, H.U., Zhang, X.C., Chen, W.T., Alam, M. and Rehman, S.U.: 2021, Reply to the comment on Zafar et al., 2020:" Petrogenesis, platinum-group element geochemistry and geodynamic evolution of Cretaceous Chilas gabbros, Kohistan island arc, NE Pakistan" by Hussain et al., 2021. Lithos, 398, 106298. DOI: 10.1016/j.lithos.2021.106298

Zafar, T., Leng, C.B., Zhang, X.C. and Rehman, H.U.: 2019a, Geochemical attributes of magmatic apatite in the Kukaazi granite from western Kunlun orogenic belt, NW China: Implications for granite petrogenesis and Pb-Zn (-Cu-W) mineralization. J of Geochem Explor, 204, 256−269. DOI: 10.1016/j.gexplo.2019.06.005

Zafar, T., Mahar, M.A., Rehman, H.U., Riaz, M., Latif, K., Oyebamiji, A. and Naeem, M.: 2019b, Geochemical and petrological characteristics of xenoliths in Mansehra Granite, NW Himalaya, Pakistan: implications for petrogenesis and tectonic settings. Episodes J of Inter Geosci, 42(4), 263−285. DOI: 10.18814/epiiugs/2019/019022

Zafar, T., Rehman, H.U., Lutfi, W., Ullah, Z., Nouri, F., Sepidbar, F. and Rehman, S.U.: 2023, Petrogenetic, geochemical, and geochronological constraints on magmatic evolution of the Chilas Complex gabbros, Kohistan arc, NW Himalaya. Geol Jour, 58(4), 1401−1427. DOI: 10.1002/gj.4665

Zafar, T., Rehman, H.U., Mahar, M.A., Alam, M., Oyebamiji, A., Rehman, S.U. and Leng, C.B.: 2020a, A critical review on petrogenetic, metallogenic and geodynamic implications of granitic rocks exposed in north and east China: New insights from apatite geochemistry. J of Geodyna, 136. DOI: 10.1016/j.jog.2020.101723

Zafar, T., Song, S., Rehman, H.U., Gamaleldien, H., Oyebamiji, A., Ullah, Z., Jadoon, U.F., Farhan, M., Khedr, M.Z., Bhat, I.M., Sepidbar, F., Nouri, F., Hussain, A., Hussain, Z. and Sami, M.: 2025, Retrieving petrogenetic source, compositional diversity and tectono-magmatic scenario of Tethyan sediment-derived magmatic flare-up: A tale from petrochemical and multi-isotopic (Sr–Nd–B–Hf) systematics. Gondwana Res. 141, 164−179. DOI: 10.1016/j.gr.2025.02.013

Zafar, T., Ur Rehman, H., Maqbool Bhat, I., Ullah, Z., Farhan, M., Oyebamiji, A. and Sami, M.: 2024, Exploring the tectono-magmatic evolution of intraoceanic fore-arc setting during subduction initiation: perspectives from trace and platinum group element systematics of the Jijal ultramafic arc system, NE Pakistan. Int Geo Rev, 66, 17, 3116−3140. DOI: 10.1080/00206814.2024.2318573

Zhang, Y., Yuan, C., Sun, M., Long, X., Wang, Y., Jiang, Y. and Lin, Z.: 2017, Arc magmatism associated with steep subduction: Insights from trace element and Sr–Nd–Hf–B isotope systematics. Jour. of Geophyl Reser: Solid Earth, 122(3), 1816−1834. DOI: 10.1002/2016JB013289

Zheng, Y-F., Xu, Z., Chen, L. Dai, L-Q. and Zhao, Z-F.: 2020, Chemical geodynamics of mafic magmatism above subduction zones. Jour of Asia Earth Sci, 194, 104185. DOI: 10.1016/j.jseaes.2019.104185